

A Comparison of Spread and Point-Source Multiple-Direction Estimation Techniques for High Latitude HF Direction Finding

by

Robert W. Jenkins

19980721 036

CRC TECHNICAL NOTE NO. 98-002

April 1998
Ottawa

The work described in this document was sponsored by the Defence R&D
Branch of the Department of National Defence under Project No. 998445419.

DISTRIBUTION STATEMENT A

Approved for public release;
Distribution Unlimited

Canada

**A Comparison of Spread and Point-Source
Multiple-Direction Estimation Techniques
for High Latitude HF Direction Finding**

by

Robert W. Jenkins

Communications Research Centre

Terrestrial Wireless Systems Research Branch

The work described in this document was sponsored by the Defence R&D
Branch of the Department of National Defence under Project No. 998445419.

INDUSTRY CANADA
CRC TECHNICAL NOTE NO. 98-002

Canada

April 1998
Ottawa

ABSTRACT

Previous simulation studies were conducted to determine the direction-finding performance of four different antenna array geometries with and without antenna pattern errors, operating with the deterministic maximum-likelihood (ML) algorithm. Here they are extended to a new DF algorithm, 'spread maximum likelihood' (SML), which assumes distributions of signal directions, rather than single directions, to approximate the signal information seen by the array. The SML algorithm is thought to be more appropriate to the high-latitude HF radio environment, where signals often arrive from a spread set of directions due to multiple reflections or scattering from irregularities in the ionosphere and, at the same time, from a single great-circle direction as a result of sporadic-E propagation. Using a performance criterion of 'point-source visibility' in the presence of a stronger spread source, the simulation shows the SML technique to yield substantially better performance than ML, for all arrays and levels of error, and array apertures of four wavelengths or more. The SML technique extended the useful range of array apertures upwards to 10 wavelengths in most cases. As was seen previously for the ML algorithm, the three-pronged star configuration was found to be best of the array geometries tested.

RÉSUMÉ

Des études antérieures exécutées à l'aide de simulations en conjonction avec l'algorithme déterministe à probabilité maximale (PM) dans lesquelles on compare quatre positions relatives d'antennes, avec ou sans l'inclusion d'erreurs de diagrammes de rayonnement, sont appliquées à un nouvel algorithme de goniométrie. Cet algorithme dit à 'probabilité maximale de dispersion' (PMD, SML en anglais pour 'spread maximum likelihood') utilise une distribution de directions de signaux plutôt que des directions simples pour établir approximativement la direction du signal incident. Cet algorithme PMD est considéré comme ayant une plus grande validité dans les régions des latitudes élevées où les signaux proviennent d'une multiplicité de directions à la suite des irrégularités de l'ionosphère et simultanément suivant la direction d'un grand cercle comme résultat de la propagation sporadique E. En utilisant une source ponctuelle (et en ligne de vue) en présence d'une source de signal diffuse comme référence de base pour l'évaluation, la simulation révèle que la méthode PMD donne un meilleur rendement que la méthode PM pour tous les réseaux d'antennes de quatre longueurs d'onde ou plus ainsi qu'à tous les niveaux d'erreurs. Dans la plupart des cas la portée des ouvertures d'antenne a été étendue jusqu'à 10 longueurs d'onde. Comme ce fut le cas pour l'algorithme PM, il a été déterminé que la configuration en étoile à trois pointes offre un rendement maximum.

EXECUTIVE SUMMARY

The high-latitude HF radio propagation environment presents a unique problem for direction finding (DF) in the form of irregular moving ionospheric patches, which reflect or scatter radio waves from many points, thus creating a multiplicity of many directions for radio signals arriving at a DF array. The signal directions span the solid angle subtended by the irregularity (spread source), and so are of little use in DF, which requires a signal direction close to the great-circle bearing from the transmitter. At the same time, an ionospheric sporadic-E layer may be present, giving rise to a single great-circle direction (point source). This point-source signal will likely be weaker than the spread-source signal from the moving ionospheric patches. The success of a DF system at such times will depend on its ability to estimate multiple directions, and to see a weak point-source direction in the presence of a distribution of many directions (spread source).

Previously conducted simulation studies of this situation compared the direction-finding performance of four different 12-element antenna array geometries, with and without antenna pattern errors, operating with the deterministic maximum-likelihood (ML) algorithm. These studies are extended here to a new DF algorithm, 'spread maximum likelihood' (SML), which employs distributions of signal directions rather than single directions, to approximate the signal information seen by the array.

The arrays were evaluated for various apertures expressed in wavelengths (which is equivalent to various operating frequencies for an array of fixed dimensions). The performance was expressed as 'point-source visibility', i.e., how much weaker a point source could be, than a neighbouring spread source, and still be seen. Performance was examined as a function of array aperture. In the previous study, for the ML algorithm, performance was limited at the large-aperture end by the limited number of signal directions assumed by the algorithm, all of which were taken up by the stronger spread source (leaving none for the point source) when the array beamwidth became too narrow as a result of the widening array aperture. The SML technique was designed to avoid this problem and to better fit the signal situation at high latitudes (spread sources and one point source).

The present modelling studies show the SML technique to perform much better than the ML technique in detecting a weak point source in the presence of a spread source, and to extend the range of useful apertures upward, to 10 wavelengths, in most cases. The three-pronged star array, which was the best performer of those tested previously with ML, was found also to be the best with the SML algorithms. The improvement in the absence of pattern errors was dramatic, and somewhat less but still substantial, when pattern errors were included. Use of the SML technique with the star array clearly extends potential DF performance to the point where the limits to performance are set primarily by antenna-pattern uncertainties.

The SML technique, by its nature, must assume a shape for the spread-signal distribution, while parameters such as mean direction and extent are adjusted to fit the observed data. Two shapes were tried: one an exact fit to the statistical average shape for spread sources modelled in the simulation, and the other significantly different. The performances in each case were similar, implying that the success of the SML technique does not depend on how closely the assumed shape fits those occurring in the signal environment at any given moment.

TABLE OF CONTENTS

ABSTRACT	iii
RESUMÉ	iii
EXECUTIVE SUMMARY	v
TABLE OF CONTENTS	vii
LIST OF FIGURES	ix
1.0 INTRODUCTION	1
2.0 BRIEF DESCRIPTION OF SPREAD MAXIMUM LIKELIHOOD TECHNIQUE	3
3.0 MODELLED SITUATION	4
4.0 RESULTS	7
4.1 AZIMUTH-TIME PLOTS AND POINT-SOURCE VISIBILITY	7
4.2 RELATIVE DF ALGORITHM PERFORMANCE FOR THE STAR ARRAY	8
4.2.1 Without Pattern Errors	9
4.2.1.1 Number of Assumed Directions	11
4.2.2 With Pattern Errors	16
4.3 RELATIVE DF ALGORITHM PERFORMANCE FOR THE OTHER ARRAYS	19
4.3.1 Without Pattern Errors	19
4.3.2 With Pattern Errors	23
5.0 SUMMARY AND DISCUSSION	30
REFERENCES	30

LIST OF FIGURES

- Figure 1. Plan views of simulated antenna arrays. 5
- Figure 2. Azimuth-time plots of estimated signal directions and spreads, found with the USML algorithm, for various point-source powers relative to the spread source, for the star array in the absence of pattern errors, and a 15° point-source/spread-source azimuthal separation. 7
- Figure 3. Point-source visibility as a function of array aperture, for the star array in the absence of antenna pattern errors, for the three modelled DF techniques: ML, ESML, and USML. 10
- Figure 4. Azimuth-time plots of estimated signal directions and spreads, found with the USML algorithm, for several numbers of assumed signal distributions for the star array in the absence of pattern errors, at a frequency of 4.0 MHz, a relative point-source power of -15 dB, and a 15° point-source/spread source azimuthal separation. 11
- Figure 5. Azimuth-time plots of estimated signal directions and spreads, found with the USML algorithm, for several numbers of assumed signal distributions for the star array in the absence of pattern errors, at a frequency of 6.0 MHz, a relative point-source power of -35 dB, and a 15° point-source/spread source azimuthal separation. 12
- Figure 6. Azimuth-time plots of estimated signal directions and spreads, found with the USML algorithm, for several numbers of assumed signal distributions for the star array in the absence of pattern errors, at a frequency of 10.0 MHz, a relative point-source power of -35 dB, and a 15° point-source/spread source azimuthal separation. 13
- Figure 7. Point-source visibility as a function of the number of assumed signal distributions, using the ESML and USML DF techniques, with the star array without antenna pattern errors, a point-source/spread-source azimuthal separation of 15° , and array apertures of 3.24, 4.86, and 8.10 wavelengths. 15
- Figure 8. Point-source visibility as a function of array aperture, for the star array in the presence of small antenna pattern errors, for the three modelled DF techniques: ML, ESML, and USML. 17
- Figure 9. Point-source visibility as a function of array aperture, for the star array in the presence of large antenna pattern errors, for the three modelled DF techniques: ML, ESML, and USML. 18

Figure 10. Point-source visibility as a function of array aperture, for the log-spiral array in the absence of antenna pattern errors, for the three modelled DF techniques: ML, ESML, and USML.	20
Figure 11. Point-source visibility as a function of array aperture, for the Vortex array in the absence of antenna pattern errors, for the three modelled DF techniques: ML, ESML, and USML.	21
Figure 12. Point-source visibility as a function of array aperture, for the centered-circle array in the absence of antenna pattern errors, for the three modelled DF techniques: ML, ESML, and USML.	22
Figure 13. Point-source visibility as a function of array aperture, for the log-spiral array in the presence of small antenna pattern errors, for the three modelled DF techniques: ML, ESML, and USML.	24
Figure 14. Point-source visibility as a function of array aperture, for the Vortex array in the presence of small antenna pattern errors, for the three modelled DF techniques: ML, ESML, and USML.	25
Figure 15. Point-source visibility as a function of array aperture, for the centered-circle array in the presence of small antenna pattern errors, for the three modelled DF techniques: ML, ESML, and USML.	26
Figure 16. Point-source visibility as a function of array aperture, for the log-spiral array in the presence of large antenna pattern errors, for the three modelled DF techniques: ML, ESML, and USML.	27
Figure 17. Point-source visibility as a function of array aperture, for the Vortex array in the presence of large antenna pattern errors, for the three modelled DF techniques: ML, ESML, and USML.	28
Figure 18. Point-source visibility as a function of array aperture, for the centered-circle array in the presence of large antenna pattern errors, for the three modelled DF techniques: ML, ESML, and USML.	29

1.0 INTRODUCTION

In developing HF direction-finding systems for use at high latitudes, it is important to consider the unique radio propagation environment present at those latitudes and to use appropriate direction-finding techniques.

The high-latitude radio propagation environment is dominated by the highly variable and irregular ionosphere present in the polar regions. During the summer, late spring and early fall months when the lower ionosphere is sunlit, photoionization provides a steady source of electrons, thereby permitting fairly stable F and E layers to exist. These layers reflect radio waves in a predictable manner, thus facilitating reliable direction finding at those times. However, during the winter months when darkness prevails, no steady electron source is present and ionospheric fluctuations dominate, causing problems for direction finding.

The earth's magnetic field lines are near vertical at high latitudes and are driven by the solar wind with the result that they follow a two-cell convection flow path, as seen from above, and are connected to solar-wind magnetic field lines within the polar cap [1-3]. In the polar cap, ionospheric electrons and positive ions travel up the magnetic field lines into the solar wind, causing a depletion of the high-latitude ionosphere during the dark winter months. The convecting magnetic field lines drag ionospheric electrons along with them, and blobs or patches of higher electron density are pulled back from the day side into the unlit night side. Occasional particle precipitation into the upper portions of the polar-cap atmosphere results in ionospheric electron density enhancements which also appear as convecting blobs or patches. These large-scale electron density enhancements cause turbulence as they convect, through the gradient-drift instability mechanism [2], giving rise to small-scale irregularities. Thus the nighttime polar-cap ionosphere is characterised by low electron densities together with irregular higher-density features convecting antisunward. Also present at times is a sporadic-E layer, possibly caused by precipitating particles.

The moving patches or blobs present during the winter months reflect or scatter HF radio waves from many points over their irregular surfaces.

A moving patch thus causes signals to arrive at a DF array from many directions, spread over the angle subtended by the patch [4, 5]. These directions, being those of the patch rather than the transmitter, are not of much use. Sporadic E, when it is present, is horizontally stratified and gives rise to great-circle radio-wave reflection. Thus sporadic E yields a signal direction representative of the transmitter bearing. The sporadic-E signals, being reflected at a lower height (100 to 120 km), arrive at lower elevation angles than the patch signals, which come from F-region heights (200 km and higher) [4]. Due to undercutting in their radiation patterns, DF antennas generally are less sensitive at low-angles, which causes the sporadic-E signals to be received with less power than the F-region patch signals. Therefore, in order to perform well at such times, a DF system must be able to see the weaker 'point-source' sporadic-E signal direction, in the presence of stronger 'spread-source' signals received from irregular F-region features.

Multiple-direction estimation techniques such as the maximum-likelihood approach allow signals from several directions to be seen at once. However, these techniques are usually limited

to resolving a small number of directions, less than the number of elements in the array. On the other hand, a spread signal source, such as that caused by a convecting F-region enhancement, has many more signal directions. The DF algorithm, in allocating its directions, will favour the stronger-signal directions, and only allocate a direction to a weaker signal when most of the stronger signals have been estimated. Thus DF algorithms which permit only a small number of signal directions to be found, may not be appropriate for high-latitude nighttime conditions.

A previous report [6] considered the performance of two multiple-direction estimators, performing in an HF propagation environment considered to be typical of high-latitude nighttime conditions. This report presented a simulation study which modelled a spread source, extended over a range of azimuths and elevations, and a weaker point source, separated in direction from the spread source by various amounts. A number of array geometries and operating frequencies were modelled, along with several levels of uncertainty in the antenna pattern information used by the DF algorithm in estimating signal directions. Initially, both the MUSIC DF algorithm and the deterministic maximum-likelihood DF algorithm were used to estimate directions. The performance criterion used to judge performance was 'point-source visibility'. This is defined as how much lower in power the point source can be below the spread signal source and still be detected as a unique signal direction. Using this criterion, the maximum-likelihood algorithm was seen to perform significantly better than MUSIC. Deterministic maximum likelihood was used for the remainder of the simulation study.

In [6], the range of operating frequencies, or array apertures measured in wavelengths over which a particular array geometry performed well, was seen to be limited on the low end by the limited resolving power of the array. On the high end it was limited by the ability of the DF algorithm to adequately describe a weak point source as well as a strong spread source with its limited number of directions. The reduced performance at the high end arises from the more narrow array beamwidth arising from the larger array aperture, which causes the DF algorithm to use more of its available direction estimates in covering the spread source, leaving none for a weak point source.

An innovation, recently developed by W. Read [7] to overcome this problem involves replacing the limited number of 'single-point' directions used by the maximum-likelihood estimator by a smaller number of distributions of directions. This approach, based upon the stochastic maximum-likelihood technique and referred to herein as the 'spread maximum-likelihood technique', is intended for situations such as that presented by the high-latitude nighttime HF propagation environment, where signals are received from a spread set of directions.

The present study extends the previous simulation study to the spread maximum-likelihood technique. The potential improvement represented by this technique is considered.

2.0 BRIEF DESCRIPTION OF SPREAD MAXIMUM-LIKELIHOOD TECHNIQUE

The spread maximum-likelihood technique was developed at DREO by W. Read, and, at the time of writing, has not been formally reported in detail. The following is a brief description of the technique, based upon provided notes [7].

The probability distribution function for a particular signal situation involving K independent signals $\hat{s}_1, \hat{s}_2, \dots, \hat{s}_K$ across the array, given a set of array measurements $\hat{x}_1, \hat{x}_2, \dots, \hat{x}_N$ representing N complex-sample vectors of dimension M taken across an array of M antennas, is given by

$$f_{\hat{x}_1, \hat{x}_2, \dots, \hat{x}_N}(\hat{s}_1, \hat{s}_2, \dots, \hat{s}_K) = \frac{1}{[(\pi)^M \det \mathbf{R}_s]^N} e^{-\sum_{i=1}^N \hat{x}_i^H \mathbf{R}_s^{-1} \hat{x}_i} \quad (1)$$

where \mathbf{R}_s is the array covariance matrix, and H denotes the conjugate transpose. Normally, the signals are assumed to each lie in a single direction, and to be uncorrelated, so that \mathbf{R}_s is given by

$$\mathbf{R}_s = \sum_{i=1}^K a_i \hat{r}_i \hat{r}_i^H \quad (2)$$

where a_i represents the power of the i th signal at the array, and \hat{r}_i represents the response vector of the array to a signal in that direction.

In order to extend this approach from a number of signals, each in a single direction, to each signal spread over its own cluster of directions, equation (2) is extended to each cluster. The resultant covariance matrix \mathbf{R}_s is given by

$$\mathbf{R}_s = \sum_{i=1}^K \mathbf{R}_i \quad (3)$$

where \mathbf{R}_i is the covariance matrix for a single spread signal. Modifying equation (2), so as to model the cluster by a set of distributed point sources, the following equation is obtained:

$$\mathbf{R}_i = a_i \sum_{j=1}^n b_j \hat{r}_j \hat{r}_j^H \quad (4)$$

where the distribution is approximated by n equally spaced directions, b_j is the fraction of the distributed signal power in the j th direction, and \hat{r}_j is the response vector of the array for the j th direction. As before, a_i is the power received by the array for the i th signal.

The number of directions n , the directions from which the array response vectors \hat{r}_j are obtained, and the distribution weights b_j are determined from the assumed distribution shape and parameters such as mean direction and extent. Two distributions were tried in the present tests: a 'rectangular' shape with a uniform power distribution over a given range of azimuths and elevations; and an 'elliptical' shape with a raised-cosine power distribution over a given range of azimuths and elevations.

3.0 MODELLED SITUATION

The present study extends the previous study of the effects of array geometry and pattern errors on high latitude DF performance [6] to the SML algorithm. A detailed description of the simulation procedure is given in that report.

The modelled signal environment is the same as in [6]: signals are scattered or reflected from many points within an irregular ionospheric patch offset from the great-circle bearing (extended source), and a weaker signal is reflected from a sporadic-E layer along the great-circle bearing (point source). The scattered signals are assumed to be uniformly distributed over a given range of elevations and azimuths ('rectangular' shape and uniform distribution). The parameters of the modelled signal environment are reproduced in Table 1. The signal powers are defined relative to a background noise level which is uncorrelated between antennas. The extended source power is set to 40 dB above the noise, while the point-source power is set to various levels, varying from 37 dB down to 5 dB above the noise.

Table 1: Parameters of Modelled Signal Environment

	case 1 15° az. separation	case 2 10° az. separation	case 3 5° az. separation
pt. source: 15° elevation, 0.5-Hz Doppler spread	180° W of N	90° W of N	270° W of N
extended source: 10 - 25° elevation, 20-Hz Doppler spread	140-165° W of N	100-125° W of N	275-300° W of N

The modelled arrays, likewise, are the same as in [6]. Four 12-element antenna geometries are used: Vortex and log-spiral geometries based on previously used actual arrays, and star and centered-circle geometries based on modelling studies. These are illustrated in Figure 1. The DF algorithms require knowledge of the antenna patterns. Three levels of pattern uncertainty are simulated, as described in the previous report [6]: no errors, small errors, and large errors. These errors are derived from antenna pattern measurements and modelling [8]. Table 2 shows the values used, for the various frequencies modelled. The small errors are typical of what is readily achieved when actual pattern measurements are used to obtain the patterns, and the large errors are typical of what is readily achieved when modelling or simple assumptions ignoring antenna interactions are used. Various operating frequencies from 2.0 to 12.0 MHz are modelled which, for the constant physical size of the arrays, correspond to array apertures from 1.62 to 9.72 wavelengths.

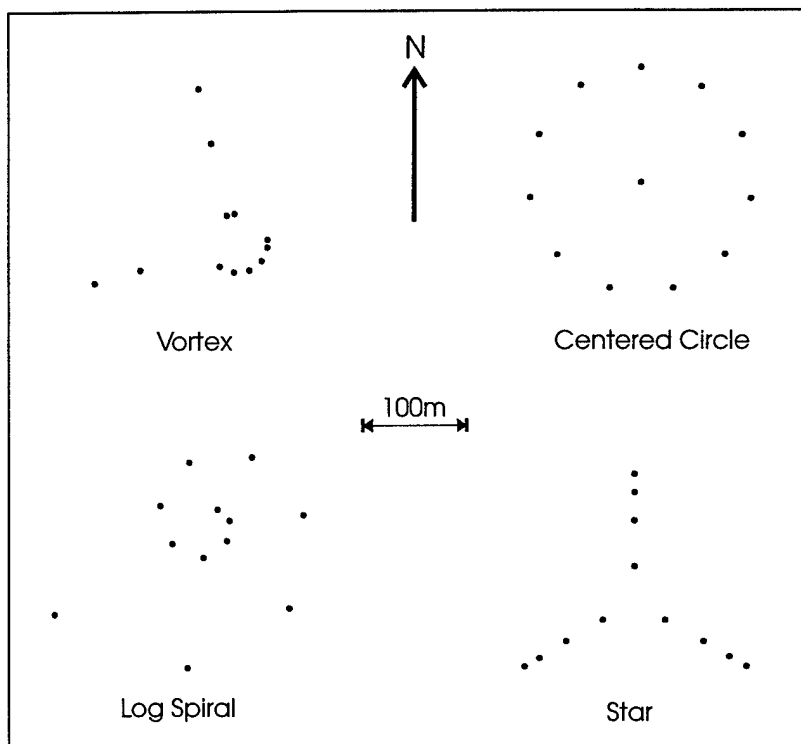


Figure 1. Plan views of simulated antenna arrays.

The DF algorithms are implemented in a form which may be applied to either previously recorded real data, or simulated data. This software package is described in an informal technical memorandum [9]. The data samples, recorded as 10 k real samples/second, are first Fourier transformed according to a 32-point transform, and the frequency containing the highest signal power selected. This process effectively presents a 312.5-Hz bandwidth filter to the received signals, thereby reducing the noise level approximately 10 dB relative to the signal. The I and Q samples from the bin containing the strongest signal are treated as complex samples which are then used to form a signal covariance matrix. Thirty-two consecutive samples are averaged to form the covariance matrix. In this way, a new covariance matrix (and resultant direction estimate) is formed every 0.1 seconds.

Table 2: RMS antenna-gain and phase-response errors simulated for the various frequencies and corresponding antenna apertures used.

frequency	aperture	small errors		large errors	
(MHz)	(wavelengths)	gain	phase	gain	phase
2.0	1.62 λ	0.19 dB	0.7°	0.58 dB	1.8°
3.0	2.43 λ	0.22 dB	1.1°	0.64 dB	2.5°
4.0	3.24 λ	0.25 dB	1.3°	0.70 dB	3.0°
5.0	4.05 λ	0.27 dB	1.6°	0.74 dB	3.5°
6.0	4.86 λ	0.29 dB	2.0°	0.78 dB	4.0°
8.0	6.48 λ	0.33 dB	2.5°	0.85 dB	5.0°
10.0	8.10 λ	0.37 dB	3.0°	0.93 dB	6.0°
12.0z	9.72 λ	0.40 dB	3.5°	1.00 dB	7.0°

The signal information in the form of the array covariance matrix is passed to the DF algorithm. In this study, three different algorithms were applied to the simulated signal information: the deterministic maximum-likelihood (ML) algorithm, used in [6], which assumes point-source signals; the spread maximum-likelihood (SML) algorithm which assumes uniform rectangular signal source distributions (USML); and the spread maximum-likelihood algorithm which assumes raised-cosine elliptical signal source distributions (ESML). The USML algorithm matches exactly the signal source distributions simulated, while the ESML algorithm represents a substantial mismatch.

As described in [6], a multi-direction estimation technique requires, as input, an estimate of the number of signal directions in order to proceed. For the ML algorithm, the AIC criterion was used [6]. At the present time, a technique for estimating the appropriate number of signal distributions for the SML algorithm has not been developed, so a number of six, equal to one-half the number of antennas in the array, was selected for most simulations. This number was intended to allow all signals present to be seen as much as possible, even with considerable mismatch between the actual and assumed signal power distributions in the extended source. At the same time, it occasionally allowed noise fluctuations and high-sidelobe features to appear as false signal directions, or caused a single spread distribution to be interpreted as a number of intertwined distributions.

Other details of the simulation process not mentioned here are described in [6]. The final results of this process is a file containing the estimated signal directions, at 0.1 second intervals,

over the duration of the simulation. For the SML algorithm, this file contains both center directions and spreads in direction for each fitted signal distribution.

4.0 RESULTS

4.1 AZIMUTH-TIME PLOTS AND POINT-SOURCE VISIBILITY

The performance criterion used in this and the previous report is 'point-source visibility', or how far the point source power can be below the spread source and have the point source still be identified as such. This criterion was selected on the basis that the great-circle direction represented by the sporadic-E point source is needed to obtain a good transmitter bearing estimate, while the bearings represented by the spread ionospheric source represent the bearing of the spread source rather than the transmitter. In [6], examples of azimuth-time resulting from the ML

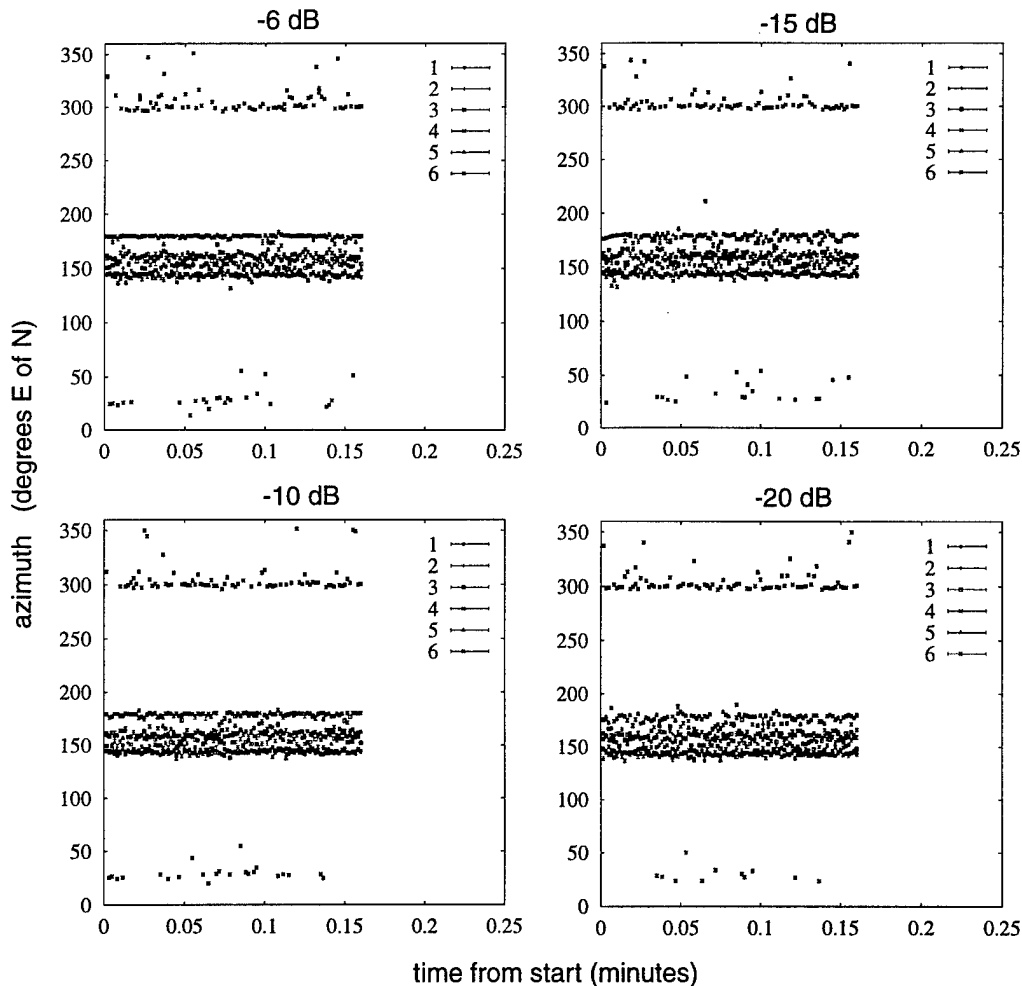


Figure 2. Azimuth-time plots of estimated signal directions and spreads, found with the USML algorithm, for various point-source powers relative to the spread source, for the star array in the absence of pattern errors, and a 15° point-source/spread-source azimuthal separation.

algorithm are shown for various relative point-source power levels, to illustrate how point-source visibility was estimated.

This section shows azimuth-time plots resulting from the SML algorithm. The plots differ from the ML plots in that both a center direction and a spread are shown for each of the estimated azimuths. Figure 2 contains azimuth-time plots, found using the USML algorithm which assumes rectangular spread distributions, for the case of the star array operating at a frequency of 4.0 MHz in the absence of pattern errors. Shown in this plot are the central locations and extents of the estimated azimuth distributions, found assuming six such distributions.

Since a relatively large fixed number (six) of signal direction distributions were assumed, false signal directions are occasionally seen, which in itself tends to limit the point-source visibility. The situation selected for Figure 2 is an example of this. The estimated azimuths tend to cover not only the spread source (140 to 165° azimuth) and the point source (180° azimuth), but also a small range of azimuths near 300°. These false directions reflect the weakest estimated signal direction, and, as will be seen in Section 4.2.1, are less in evidence when fewer signal directions are assumed.

Although the spread-source distributions used by the USML algorithm were an exact match to those simulated by the signal model (in the statistical sense), the spread source is not described in the resulting plots as a single spread source with a spread extending from 140° to 165° azimuth. Instead, since there are more than enough signal directions to model this and the point source, some of the directions go into modelling the statistical fluctuations in the spread source shape, with the result that it is seen as a scattered set of much narrower distributions (almost points) distributed fairly uniformly between 140° and 165° azimuth. Reducing the number of assumed directions causes the spread source to be modelled by fewer wider distributions more representative of the spread nature of this source; at the same time it may cause some reduction in the sensitivity of the algorithm to a much weaker point source. This issue is explored more fully in Section 4.2.1.1.

From Figure 2, the point source is seen clearly, when its power is -6 dB relative to the spread source, as a distinct well-defined narrow set of directions. As the point source's power is reduced, its trace becomes broader and less well defined until, at -20 dB, it has started to merge with the spread-source trace. Even at this stage, however, it remains stronger than the false trace at 300° azimuth. The point-source visibility, or relative power at which the point source ceases to be identified as a point source, was estimated from these plots to be approximately -17 dB in this case. The uncertainty in this estimate and other such estimates is considered to be 1 or 2 dB.

4.2 RELATIVE DF ALGORITHM PERFORMANCE FOR THE STAR ARRAY

Previously, it was shown that with the deterministic maximum-likelihood approach, the best array performances of the four array geometries were achieved by the star array. In this section, the performances of this array using the spread maximum-likelihood algorithm are examined and compared to those obtained previously.

4.2.1 Without Pattern Errors

Figure 3 compares performances of the ML, ESML, and USML algorithms for the star array. Point-source visibility is plotted as a function of array aperture, for the three modelled spread-source/point-source azimuthal separations: 5° , 10° and 15° .

The limits on point-source visibility are discussed in [6], for the deterministic maximum-likelihood (ML) algorithm which approximates the situation with a few single directions. For smaller array apertures, the poor resolving power limits the point-source visibility in the presence of a stronger spread source. For large array apertures, the limit to performance is set by the narrowness of the array beamwidth relative to the spread source, and by the resulting greater number of directions required to describe the spread source before a direction can be allocated to the weaker point source. The best array performances were achieved between these limits.

The spread maximum-likelihood (SML) algorithm, in replacing estimated (single) directions with estimated distributions of directions, is expected to overcome the high-aperture limit. The results displayed in Figure 3 confirm these expectations. With the ML algorithm, the point-source visibility is poor for small array apertures, improves as the aperture is increased to an optimum value (e.g., -24 dB at 5 wavelengths, for a point-source/extended-source separation of 15°) and then worsens as the aperture is further increased.

When the ML algorithm is replaced by either the ESML or USML algorithms, there is a marked improvement in performance for larger apertures. While the performance for the small apertures is somewhat worse, it becomes significantly better for the apertures that previously displayed the best performance, especially so at the largest apertures. The aperture showing the best performance is increased (e.g., for a separation of 15° , from 5 wavelengths to 6.5 wavelengths), and the actual performance is improved, sometimes dramatically (e.g., for 15° separation, from -24 dB to -38 dB).

It might be expected that the USML algorithm, with its assumed spread-direction distribution similar to that modelled, would yield better results than the ESML algorithm whose assumed direction distribution is significantly different. However, in Figure 3, no significant difference in performance is noted. The number of assumed direction distributions being larger than the number of sources actually present does tend to compensate for the mismatch between the assumed elliptical raised-cosine distributions of ESML and the modelled rectangular uniform-source shape, since a number of distributions can be combined to better describe a differently shaped distribution.

While the improvements described above are most dramatic for the largest point-source/spread-source separation (15°), they also apply to the smaller separations of 10° and 5° azimuth. For the 10° and 15° separations, an improvement in point-source visibility of the order of 15 to 20 dB is achieved for the star array geometry with apertures larger than 5 wavelengths. For 5° separation, the improvement is of the order of 5 to 10 dB.

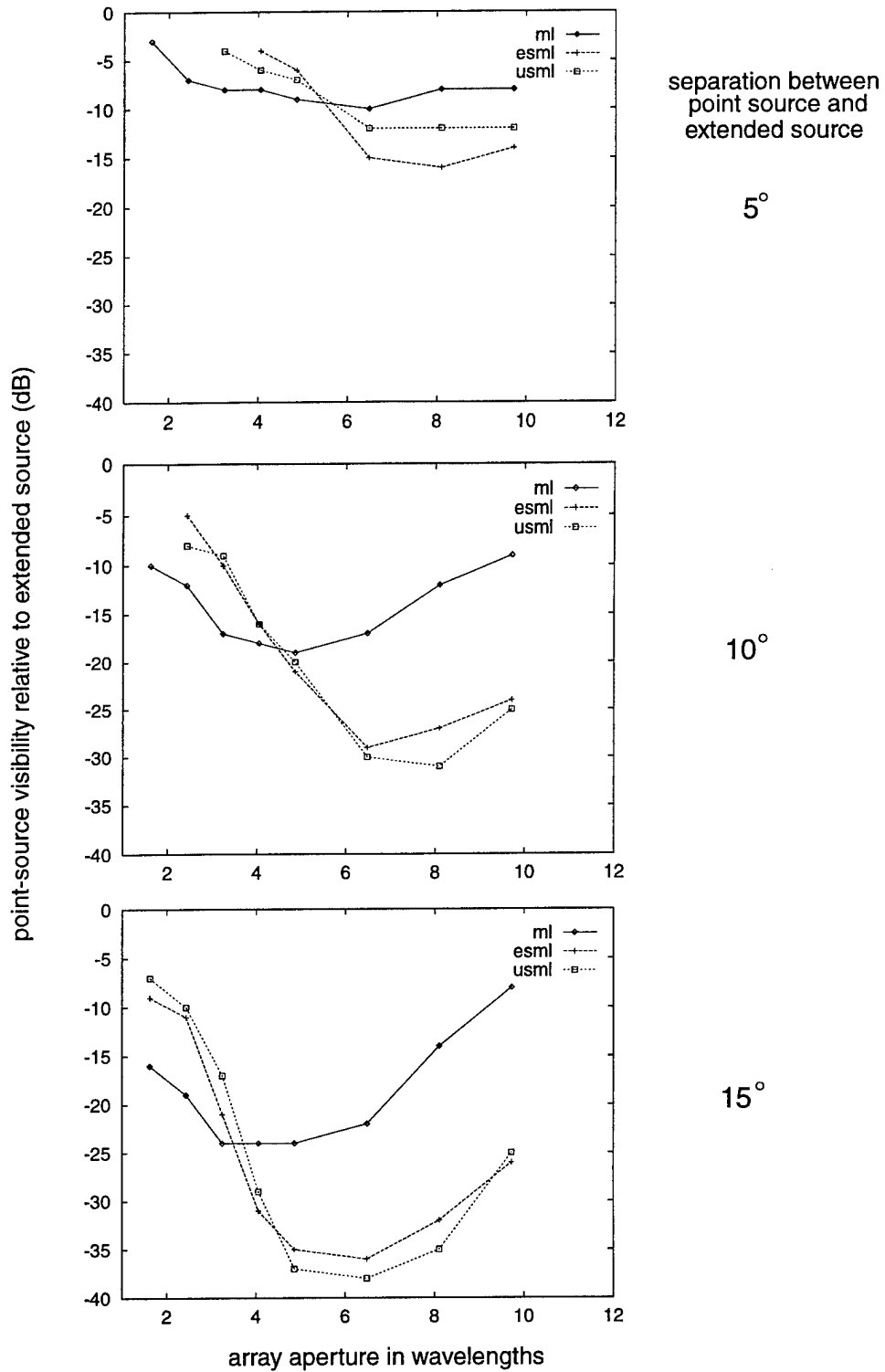


Figure 3. Point-source visibility as a function of array aperture, for the star array in the absence of antenna pattern errors, for the three modelled DF techniques: ML, ESML, and USML.

4.2.1.1 Number of Assumed Directions

The effect of changing the number of assumed directions was investigated for a limited number of situations: in particular, for the star array without pattern errors, in the presence of a 15° point-source/spread-source separation. Frequencies of 4.0, 6.0, and 10.0 MHz, corresponding to array apertures of 3.24, 4.86 and 8.10 wavelengths, were selected for this study. Both the ESML and USML algorithms were tested.

Figure 4, 5, and 6 show azimuth-time plots, for 4.0-, 6.0-, and 10.0-MHz frequencies, respectively, for the USML algorithm, each at a signal level where the point source was becoming hard to see, for 2, 3, 4 and 5 assumed signal distributions.

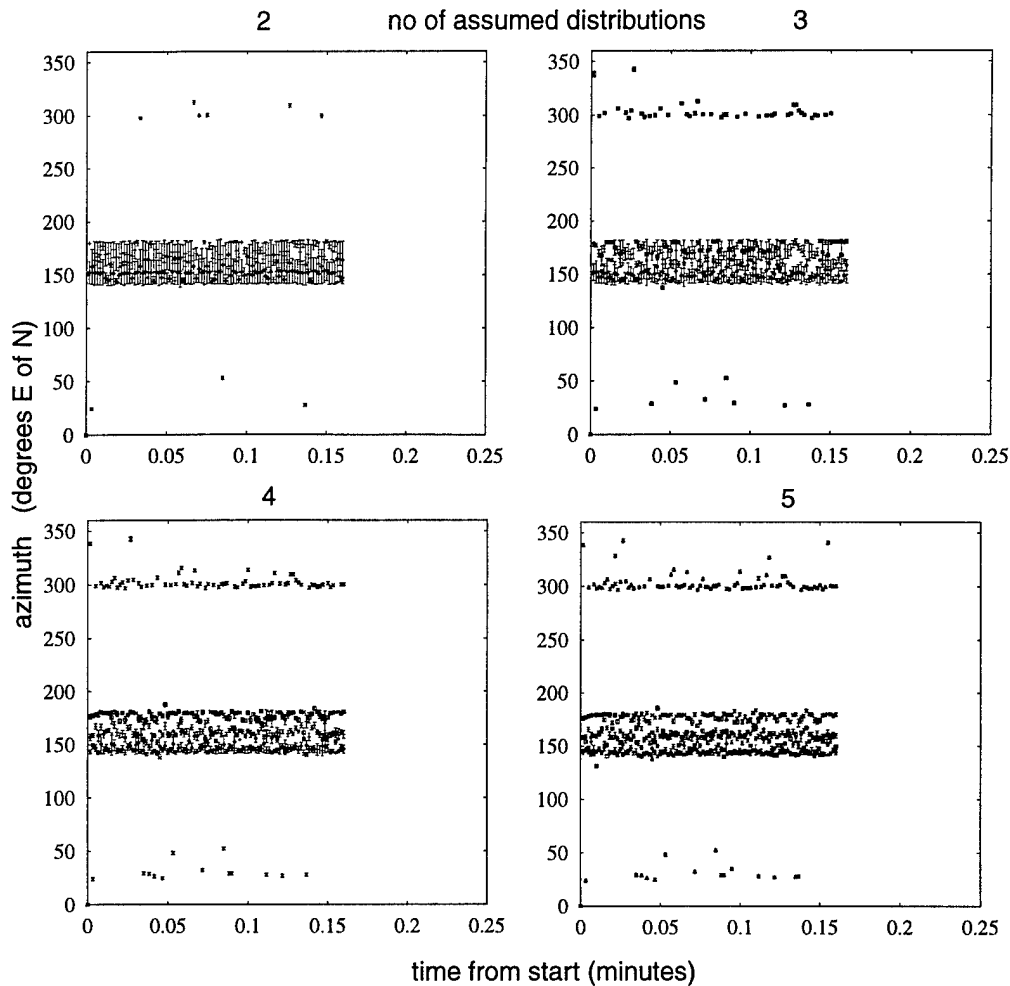


Figure 4. Azimuth-time plots of estimated signal directions and spreads, found with the USML algorithm, for several numbers of assumed signal distributions for the star array in the absence of pattern errors, at a frequency of 4.0 MHz, a relative point-source power of -15 dB, and a 15° point-source/spread-source azimuthal separation.

is not quite visible with the number of assumed directions set to three, and barely visible with four or five assumed directions. In Figure 2, the point source at -15 dB is just barely visible for six assumed directions. In each case where the point source is seen (four, five, or six assumed directions) the false trace at 300° azimuth is fairly strong. In each of these cases, the false trace is formed from the weakest of the distributions to be fitted. The spread source for these cases is also seen as a collection of smaller disjoint spread sources, rather than a single source.

Figures 5 and 6, for 6.0 and 10.0 MHz corresponding to apertures in the medium-to-large range of those investigated (4.86 and 8.10 wavelengths respectively), are similar in their displayed results. Both these cases have a point-source power of -35 dB relative to the spread source and, as can be seen in Figure 3, the apertures are large enough that the performance is not significantly limited by the resolving power of the array.

For 6.0 MHz (Figure 5), the spread source and point source are readily identified by assuming just two distributions. As the number of distributions is increased, the spread source begins to be represented by several disjoint distributions rather than a single distribution, the point source is more visible, and false directions become weakly visible.

The same behaviour is seen for 10.0 MHz (Figure 6). In this case, the point-source visibility is slightly lower. When only two distributions are assumed, the point source is not visible. Both distributions go into describing the spread source (likely as a result of the statistical fluctuations from the average in the shape of the actual spread source). When the number of assumed distributions is increased to three and beyond, the point source becomes weakly visible. A few scattered false directions are also seen as the number of directions is increased, but they do not form significant traces.

The effect of the number of assumed signal distributions on point-source visibility is presented in Figure 7, for 4.0, 6.0 and 10.0 MHz, and a point-source/spread-source separation of 15° in azimuth. The 4.0-MHz frequency, as stated previously, corresponds to a relatively small aperture, where the point-source visibility is limited by the ability of the array to resolve directions. At this frequency, the USML and ESML algorithms perform similarly, even when only two signal distributions are assumed. As the number of assumed distributions is increased, the performance of both algorithms improves, with the ESML showing slightly better behaviour than USML for three or more assumed distributions.

The 6.0- and 10.0-MHz frequency plots in Figure 7 show the USML and ESML algorithms to perform equally well when three or more signal directions are assumed; their performances remain very good and vary only slightly in going from three to six assumed distributions, achieving the best performance with four assumed distributions, and deteriorating only slightly, if at all, as the number of assumed distributions is increased to six. However, when only two directions are assumed, the ESML algorithm performance worsens dramatically for 6.0 MHz and less for 10.0 MHz, while the USML performance remains unchanged.

These results suggest that a misfit, between the assumed signal distribution shape and

those

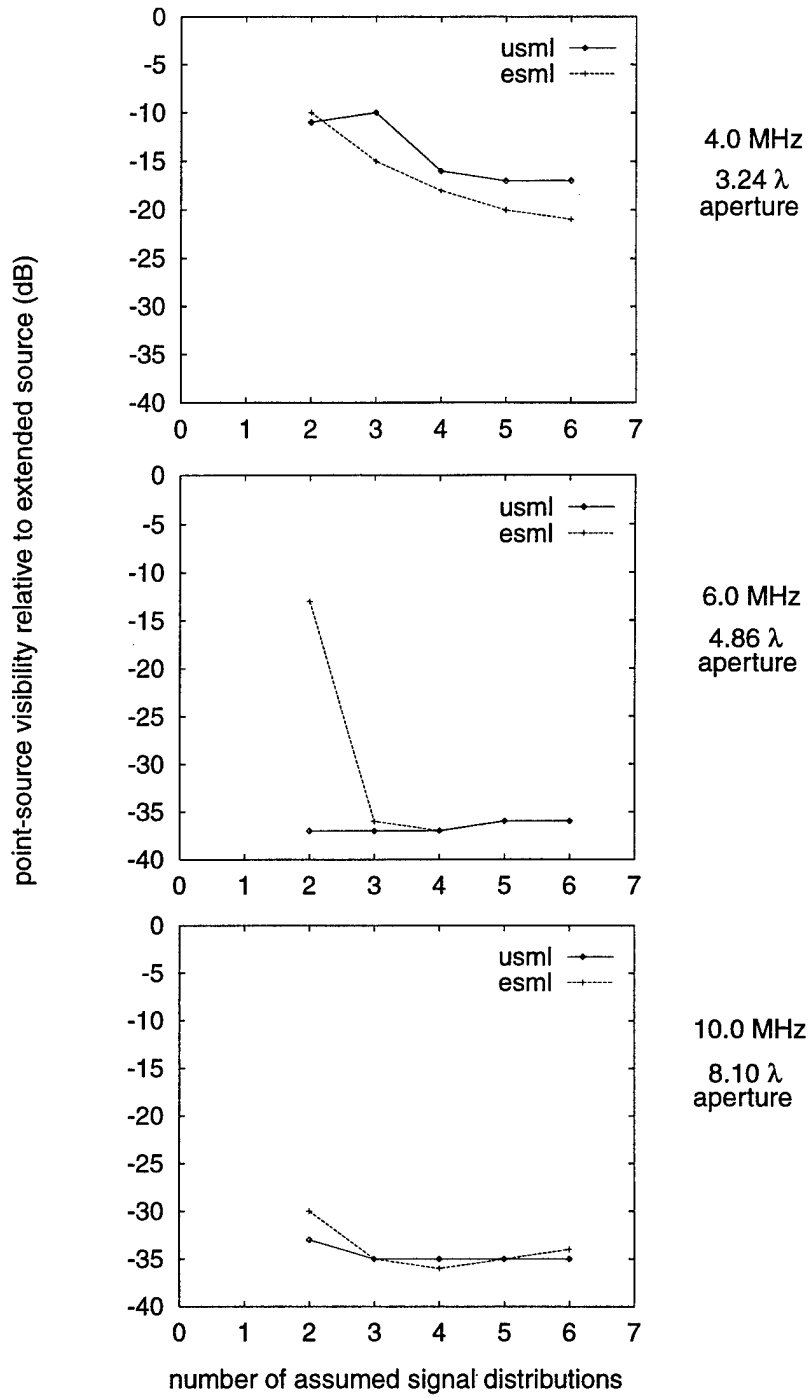


Figure 7. Point-source visibility as a function of the number of assumed signal distributions, using the ESML and USML DF techniques, with the star array without antenna pattern errors, a point-source/spread-source azimuthal separation of 15° , and array apertures of 3.24, 4.86, and 8.10 wavelengths.

shapes actually present in the signal data, presents a problem only when the number of assumed directions matches the number of signals. Mismatch problems can be avoided by using a number of assumed directions somewhat greater than the number of signal distributions anticipated in the data. When this is done, however, spread sources tend to appear as several randomly intertwined disjoint smaller-spread sources. At small apertures, increasing the number of assumed distributions makes it easier to resolve a weak point source from a nearby spread source. From the above observations, it appears that the assumption of six signal distributions used for most of the simulations represents a reasonable choice for the cases tested.

4.2.2 With Pattern Errors

Figures 8 and 9 show the corresponding results for the star array, for small and large antenna pattern errors, respectively. As before, point-source visibility is plotted as a function of array aperture in wavelengths, and plots are included for the three point-source/spread-source azimuthal separations: 5° , 10° , and 15° . Curves for the ML, ESML, and USML DF techniques are included in each of the plots.

Previously [6], it was seen that for the ML technique, the introduction of pattern errors reduced array performance, more so at the smaller apertures. This can also be seen to be the case for the SML techniques, by comparing Figure 3 with Figures 8 and 9. Moreover, antenna-pattern errors reduce the amount by which the point-source visibility of the SML techniques exceeds that achieved with the ML technique. A substantial performance reduction occurs at large apertures as well as small apertures: apparently the very good performance noted at large apertures for the SML techniques is very sensitive to pattern errors.

Nonetheless, even with pattern errors, the two SML techniques perform noticeably better than the ML technique for moderate and large array apertures. The SML techniques result in a point-source visibility for the star array, with small pattern errors, that is approximately 12 dB better than that of the ML array at 15° point-source/spread-source separation; 5 to 7 dB better at 10° separation; and 2 or 3 dB better at 5° separation. With large errors, the point-source visibility with the two SML techniques is 5 or 6 dB better at 15° separation; 4 or 5 dB better at 10° separation; and 1 or 2 dB better at 5° separation.

Just as when there are no pattern errors, the ESML and USML techniques perform approximately equally well in the presence of pattern errors, despite the fact that only the USML technique uses signal distributions identical to those simulated in the data.

From these observations, it can be concluded that, for the star array geometry, the SML algorithms exhibit substantially better performance than the ML algorithm, in revealing a well-defined weak signal in the presence of a stronger spread signal. However, to take best advantage of the improvement in performance, it is important to know the antenna patterns of the DF array as accurately as possible.

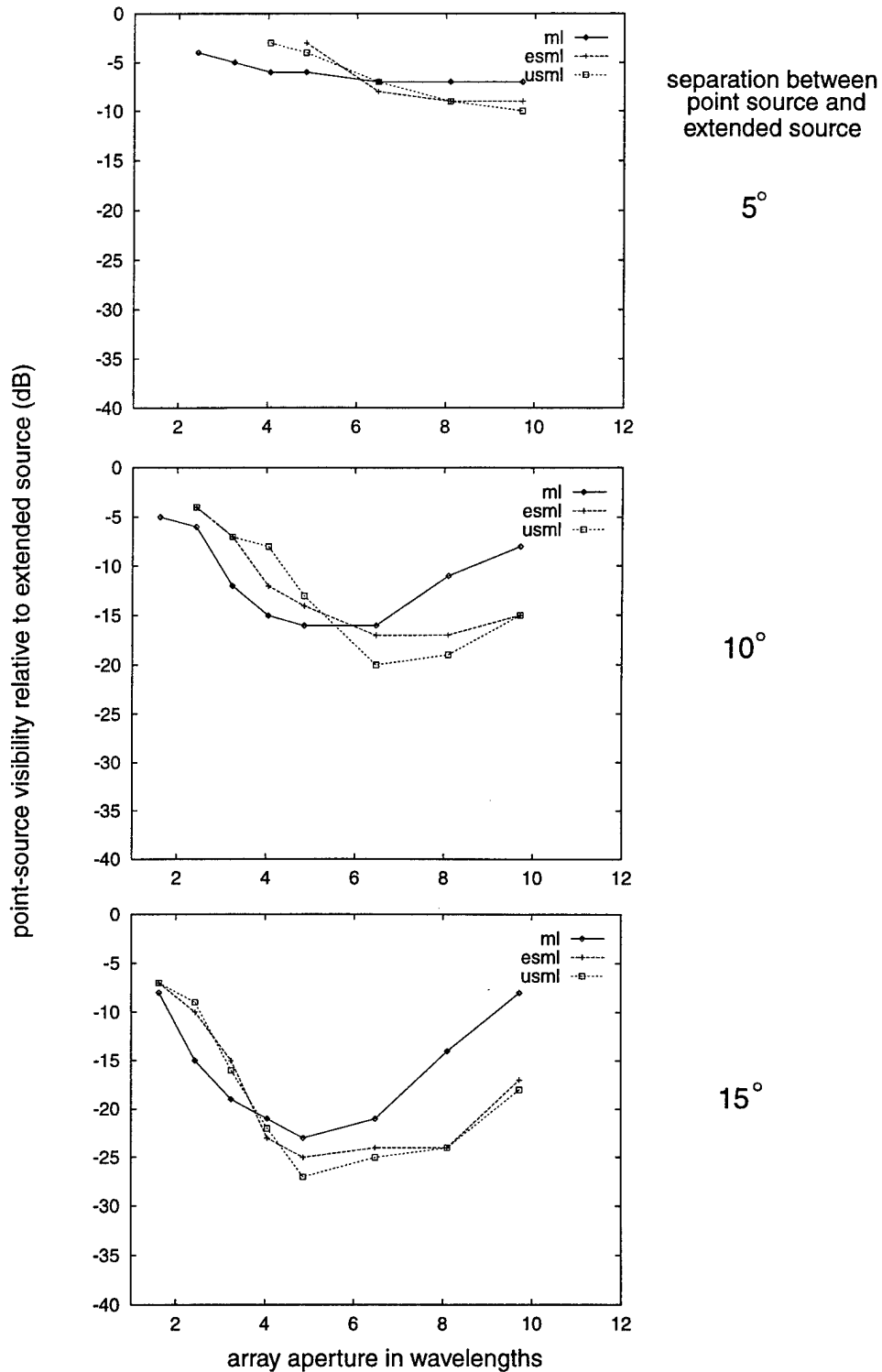


Figure 8. Point-source visibility as a function of array aperture, for the star array in the presence of small antenna pattern errors, for the three modelled DF techniques: ML, ESML, and USML.

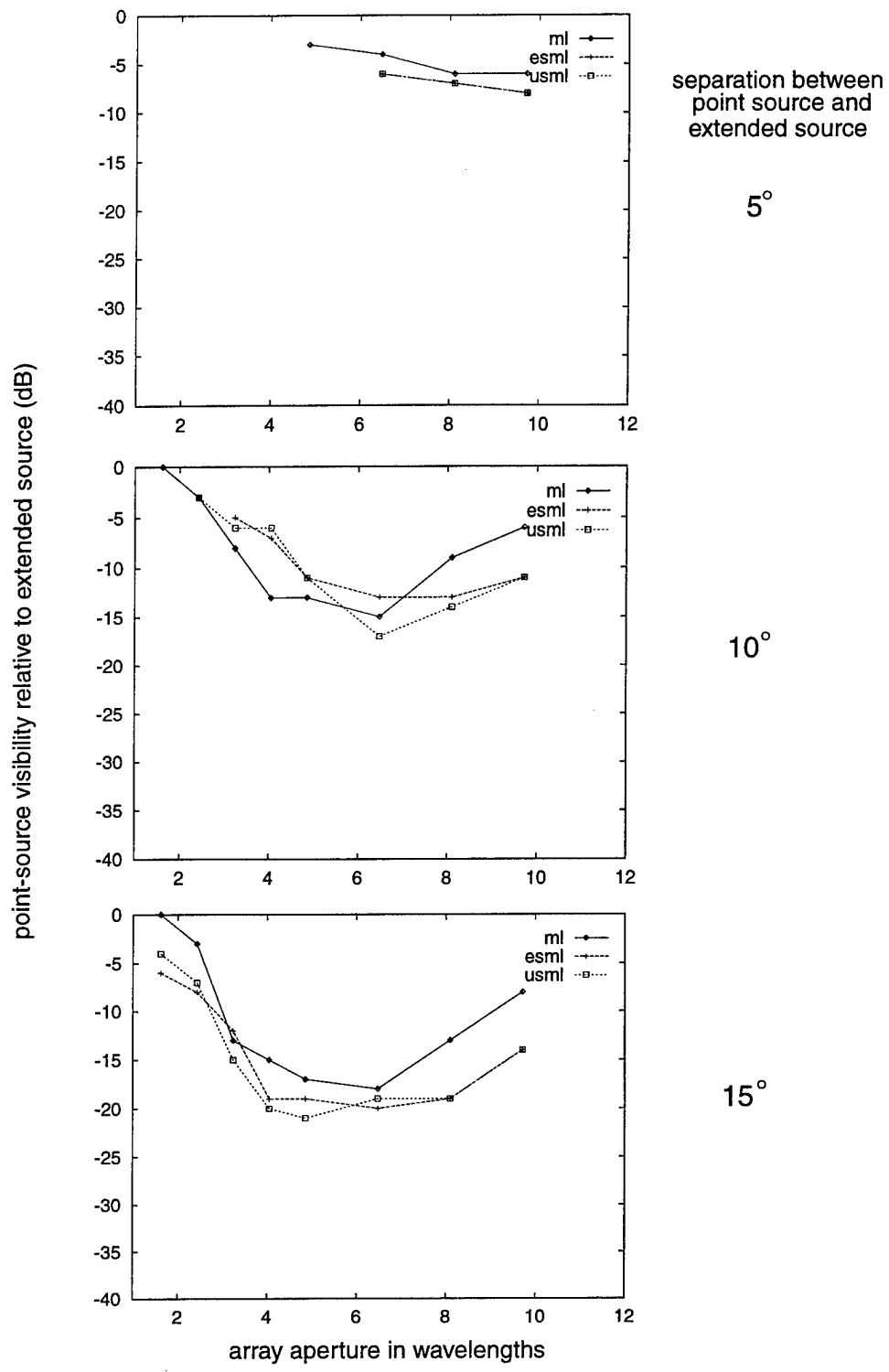


Figure 9. Point-source visibility as a function of array aperture, for the star array in the presence of large antenna pattern errors, for the three modelled DF techniques: ML, ESML, and USML.

4.3 RELATIVE DF ALGORITHM PERFORMANCE FOR THE OTHER ARRAYS

4.3.1 Without Pattern Errors

Figures 10, 11 and 12 show the DF performances in the absence of antenna pattern errors, of the log-spiral, Vortex and centered-circle arrays, respectively. As before, point-source visibility is plotted as a function of array aperture, in each plot, for the three DF techniques: ML, ESML and USML. Plots are provided in these figures for each of the three point-source/spread-source separations modelled. These figures, along with Figure 3 for the star array, are considered in this section.

The ESML and USML techniques were noted in Section 4.2.1 to improve performance dramatically for the star array at apertures of 5 wavelengths and higher, in the absence of pattern errors. The same dramatic improvement is seen to occur for the log-spiral and Vortex arrays, in Figures 10 and 11. A significant improvement is also noted for the centered-circle array in Figure 12, but is limited to apertures between 4 and 7 wavelengths. For the log-spiral and Vortex arrays, the useful array aperture is extended upward to almost 10 wavelengths and, for the centered-circle array, to approximately 6 wavelengths.

Previously [6], the star array was noted to have the best performance of the four arrays with the ML technique. From Figures 3, 10, 11 and 12, this array is noted to be the best performer with SML as well. For example, at 15° separation, the star array with SML techniques achieves a point-source visibility of -38 dB at its best aperture, and a visibility better than -20 dB over apertures from roughly 3.5 to more than 10 wavelengths. In comparison, the log-spiral array achieves a best point-source visibility of only -26 dB, and exceeds -20 dB visibility from 3 to 9.5 wavelengths aperture; the Vortex array achieves a best point-source visibility of -32 dB and exceeds a visibility of -20 dB between 3 and 10 wavelengths aperture, and the centered-circle array achieves a point-source visibility of -30 dB and exceeds -20 dB visibility for apertures between 2.5 and 6 wavelengths.

Figures 10, 11 and 12 reveal that the ESML and USML algorithms have similar performances, when used with the log-spiral, Vortex, and centered-circle arrays respectively, as they do with the star array.

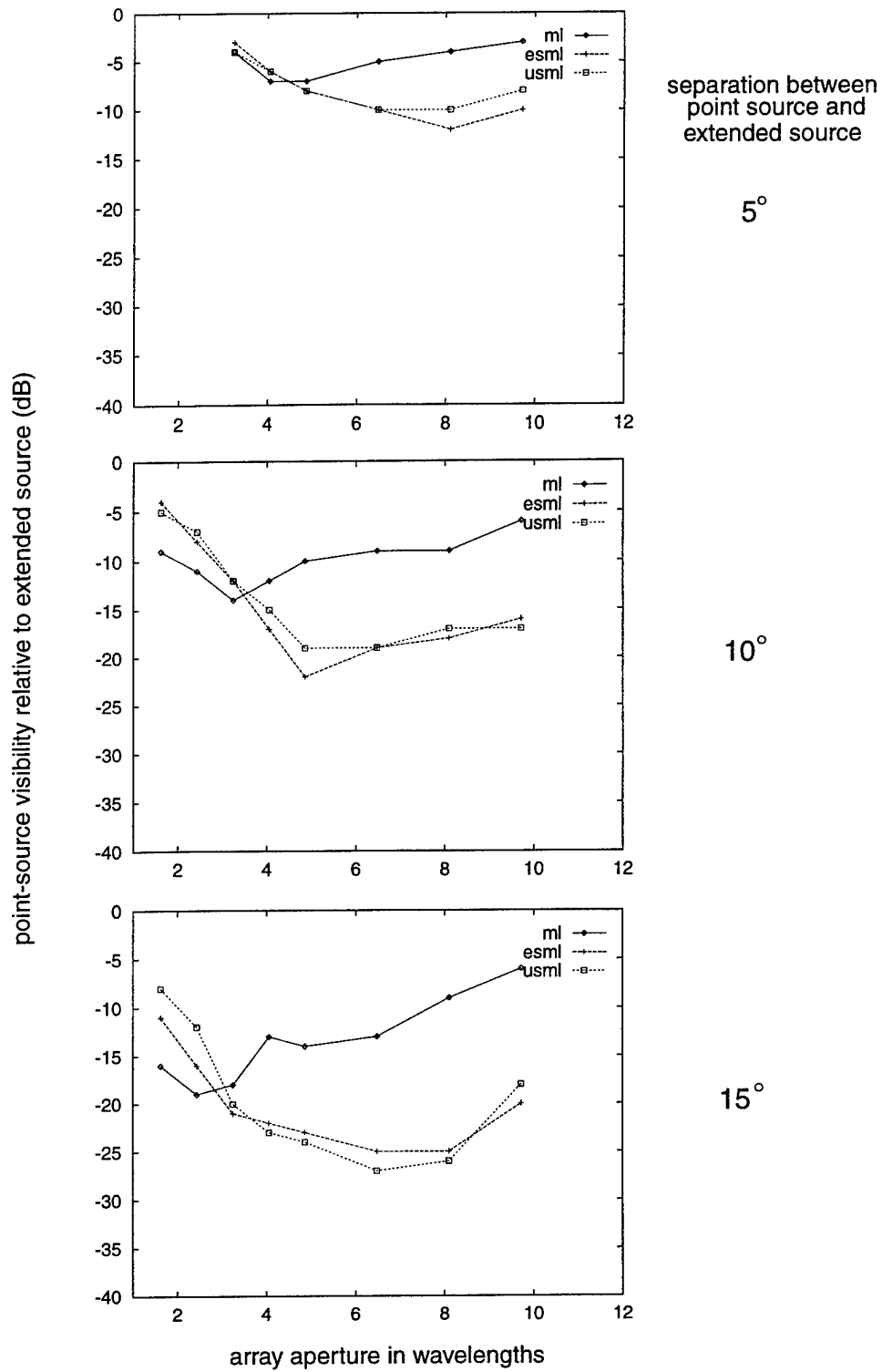


Figure 10. Point-source visibility as a function of array aperture, for the log-spiral array in the absence of antenna pattern errors, for the three modelled DF techniques: ML, ESML, and USML.

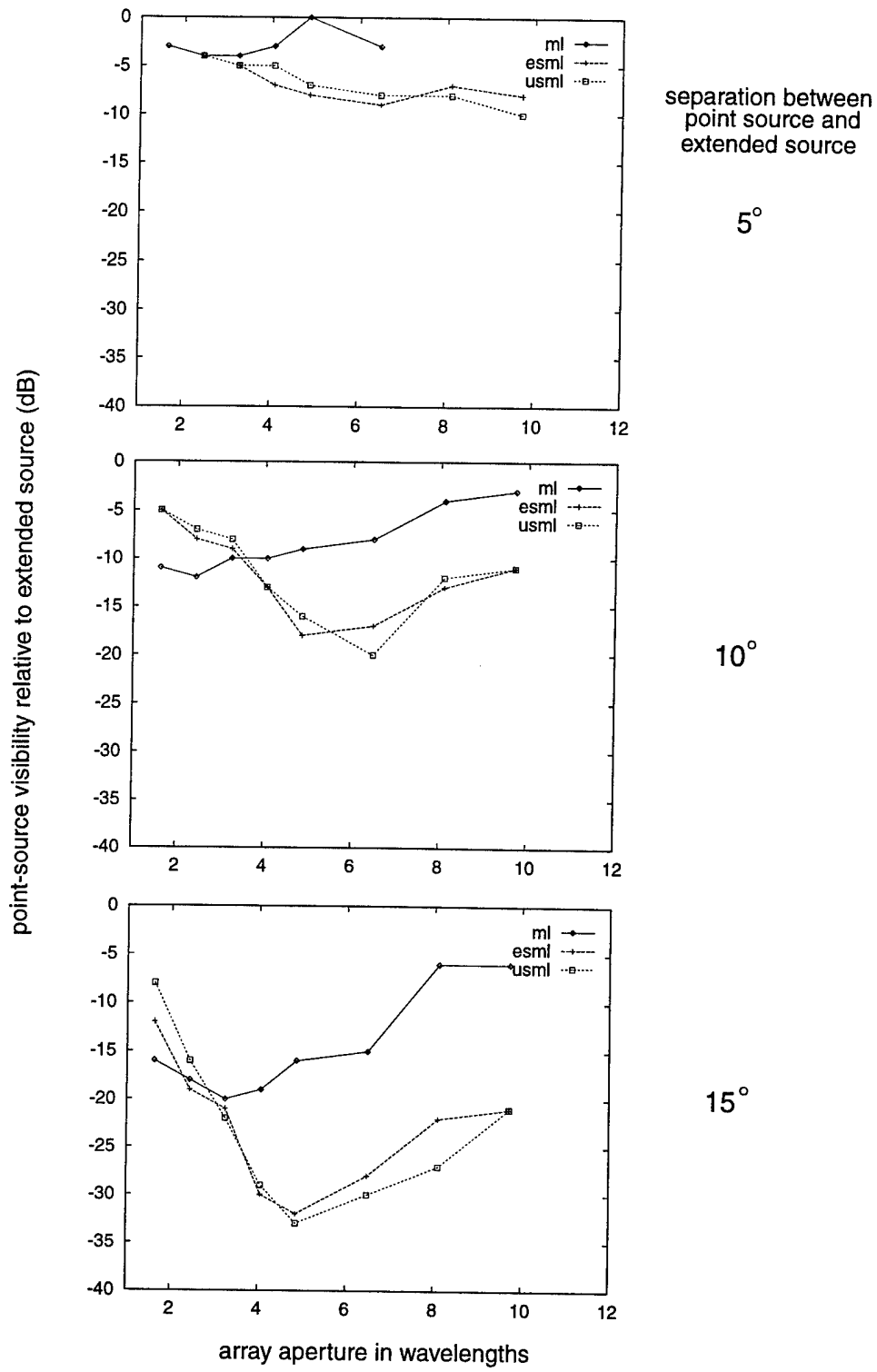


Figure 11. Point-source visibility as a function of array aperture, for the Vortex array in the absence of antenna pattern errors, for the three modelled DF techniques: ML, ESML, and USML.

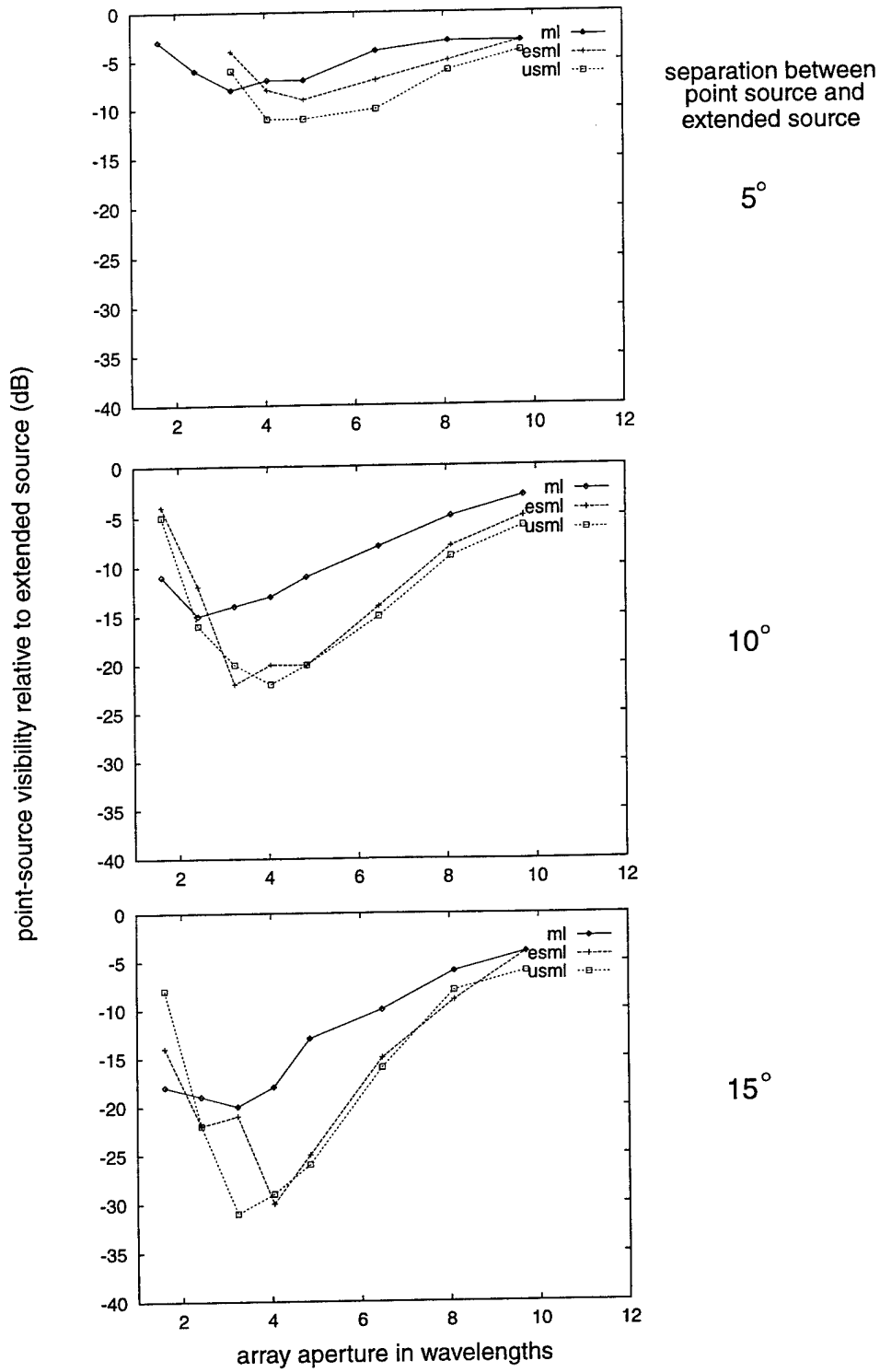


Figure 12. Point-source visibility as a function of array aperture, for the centered-circle array in the absence of antenna pattern errors, for the three modelled DF techniques: ML, ESML, and USML.

4.3.2 With Pattern Errors

Figures 13, 14, and 15 compare the performances of the ML, ESML, and USML algorithms for the log-spiral, Vortex, and centered-circle arrays, respectively, with 'small' modelled pattern errors (Table 2). These figures can be compared with Figure 8, showing the performance of the star array with small pattern errors. Figures 16, 17, and 18 provide a similar comparison, with large pattern errors, for the log-spiral, Vortex and centered-circle arrays, respectively, and can be compared with Figure 9 for the star array with large errors.

In Section 4.2.2, where the star array geometry was used, it was helpful to compare the performances achieved with errors to those without, both in terms of the actual performances and in terms of the improvements noted in going from the ML to the SML techniques. The same is done here, for each of the other three array geometries.

The effect of pattern errors on the performance of the log-spiral array operating with the SML algorithms can be seen by examining Figures 10, 13 and 16. The introduction of pattern errors reduces the amount by which the SML algorithms perform better than the ML algorithm, with this array, but not as much as for the star array, which has a better performance in the absence of errors, and so has more to lose with the introduction of errors. Even with large errors, however, the SML algorithms perform noticeably better at all but small apertures, for all three separations.

Figures 11, 14, and 17 illustrate the effect of pattern errors on performance of the Vortex array geometry. The introduction of pattern errors significantly reduces the amount by which the SML algorithms perform better than the ML algorithm, perhaps more than was noted for the log-spiral array. Again, even with large errors, the SML algorithms perform better than ML at all but small apertures.

The effect of pattern errors on SML performance with the centered-circle array is illustrated in Figures 12, 15, and 18. This array geometry, even with the SML algorithms, is more limited in its useful aperture range than the other geometries. Again, the addition of errors reduces the amount by which the SML algorithms increase performance over that of the ML algorithm. Even with large errors, the SML algorithms continue to perform better than the ML algorithm, except at small apertures (4 wavelengths or less) and, in this case, the largest tested apertures (above 7 wavelengths) where this array does not perform well.

As was the case without pattern errors, no significant differences in performance between the ESML and USML algorithms are noted for any of the four array geometries tested.

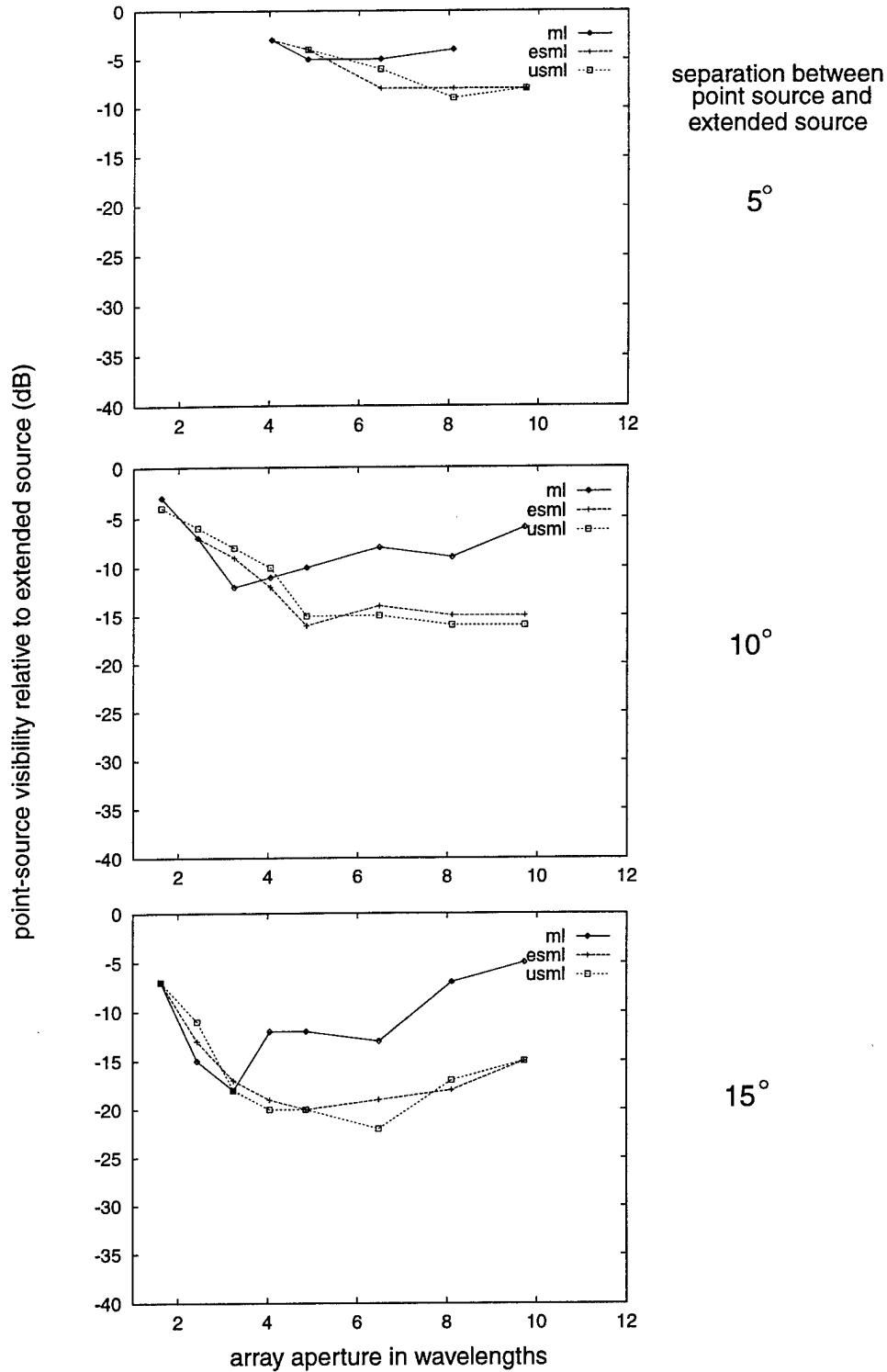


Figure 13. Point-source visibility as a function of array aperture, for the log-spiral array in the presence of small antenna pattern errors, for the three modelled DF techniques: ML, ESML, and USML.

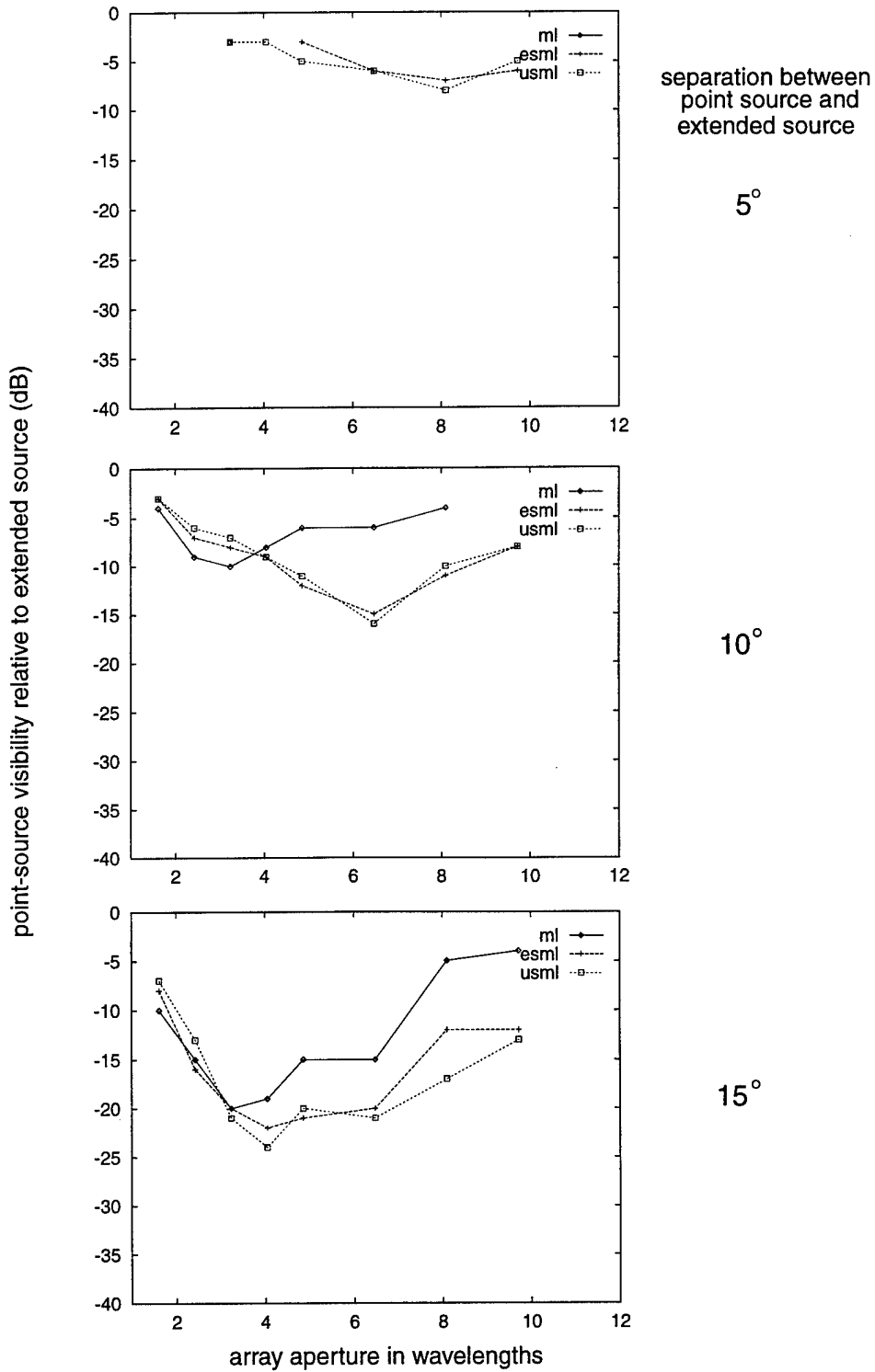


Figure 14. Point-source visibility as a function of array aperture, for the Vortex array in the presence of small antenna pattern errors, for the three modelled DF techniques: ML, ESML, and USML.

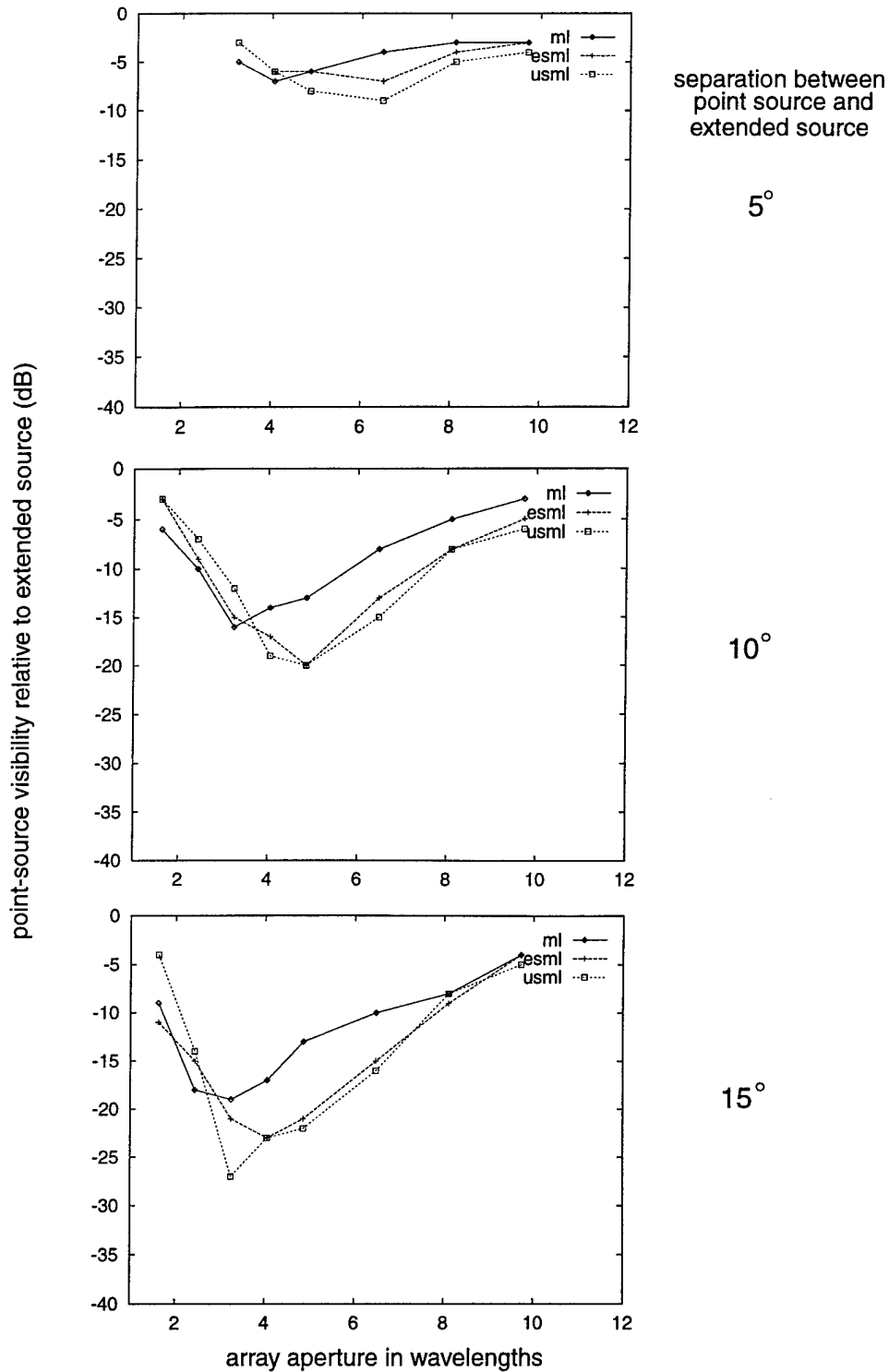


Figure 15. Point-source visibility as a function of array aperture, for the centered-circle array in the presence of small antenna pattern errors, for the three modelled DF techniques: ML, ESML, and USML.

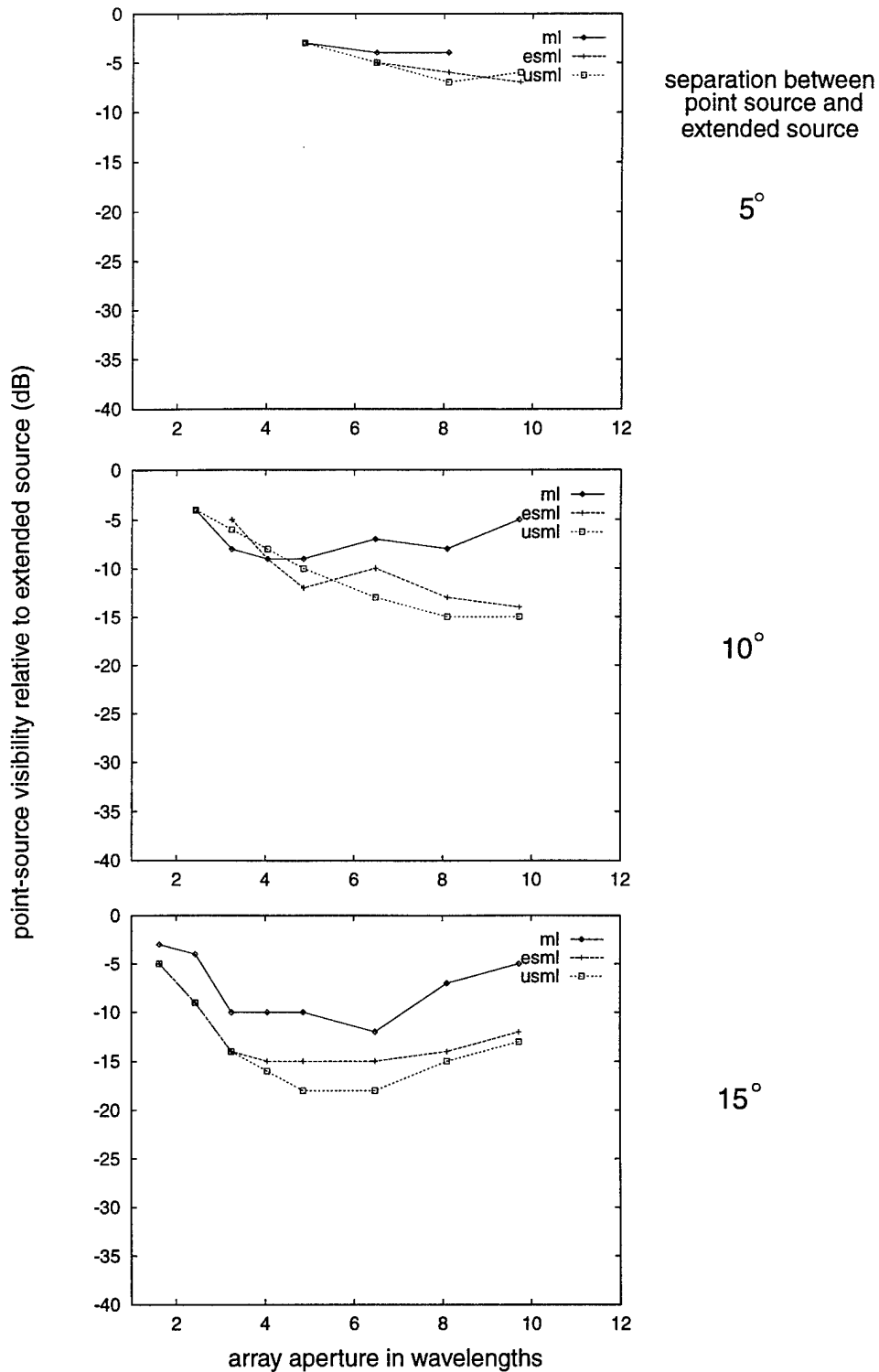


Figure 16. Point-source visibility as a function of array aperture, for the log-spiral array in the presence of large antenna pattern errors, for the three modelled DF techniques: ML, ESML, and USML.

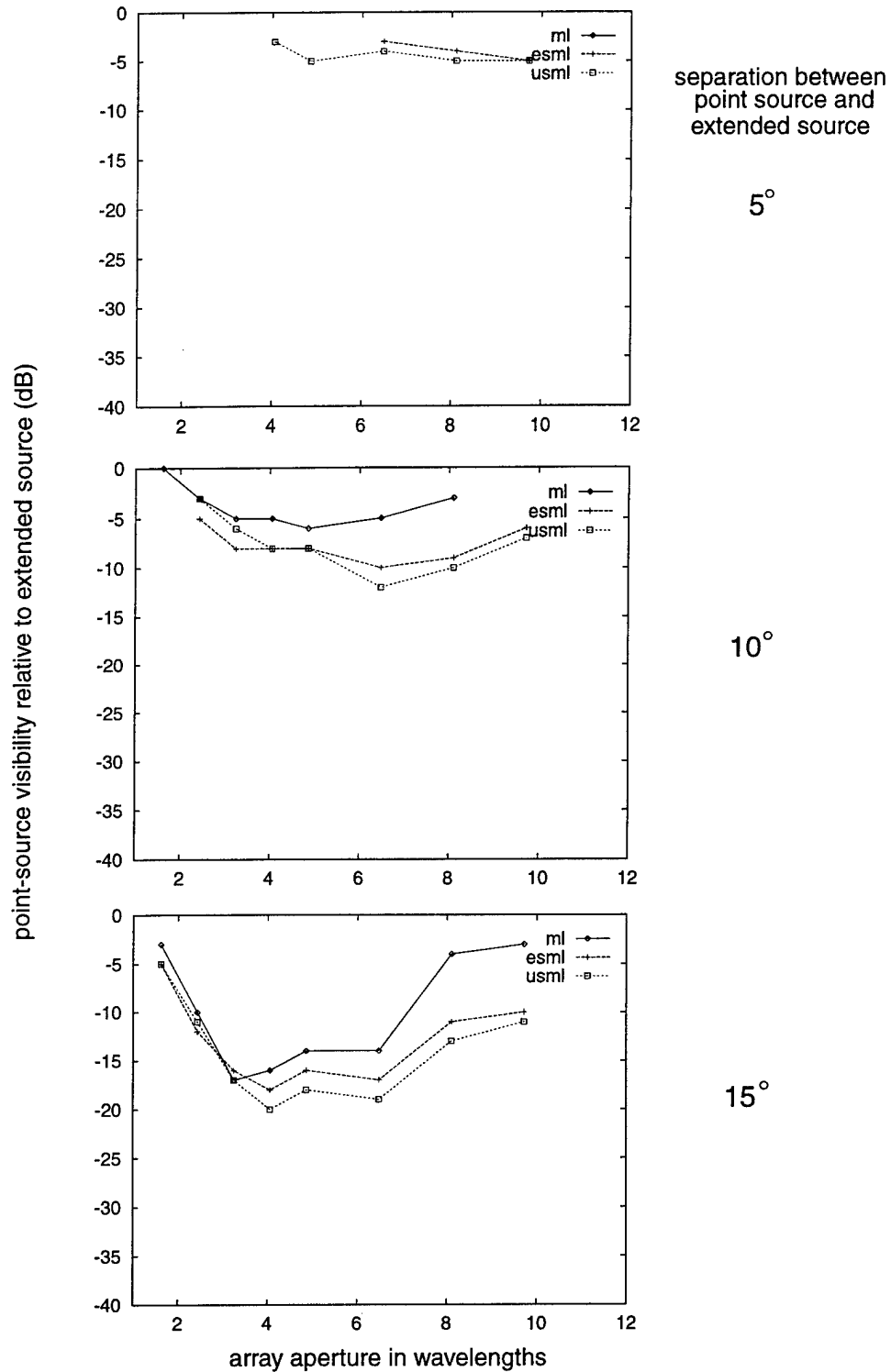


Figure 17. Point-source visibility as a function of array aperture, for the Vortex array in the presence of large antenna pattern errors, for the three modelled DF techniques: ML, ESML, and USML.

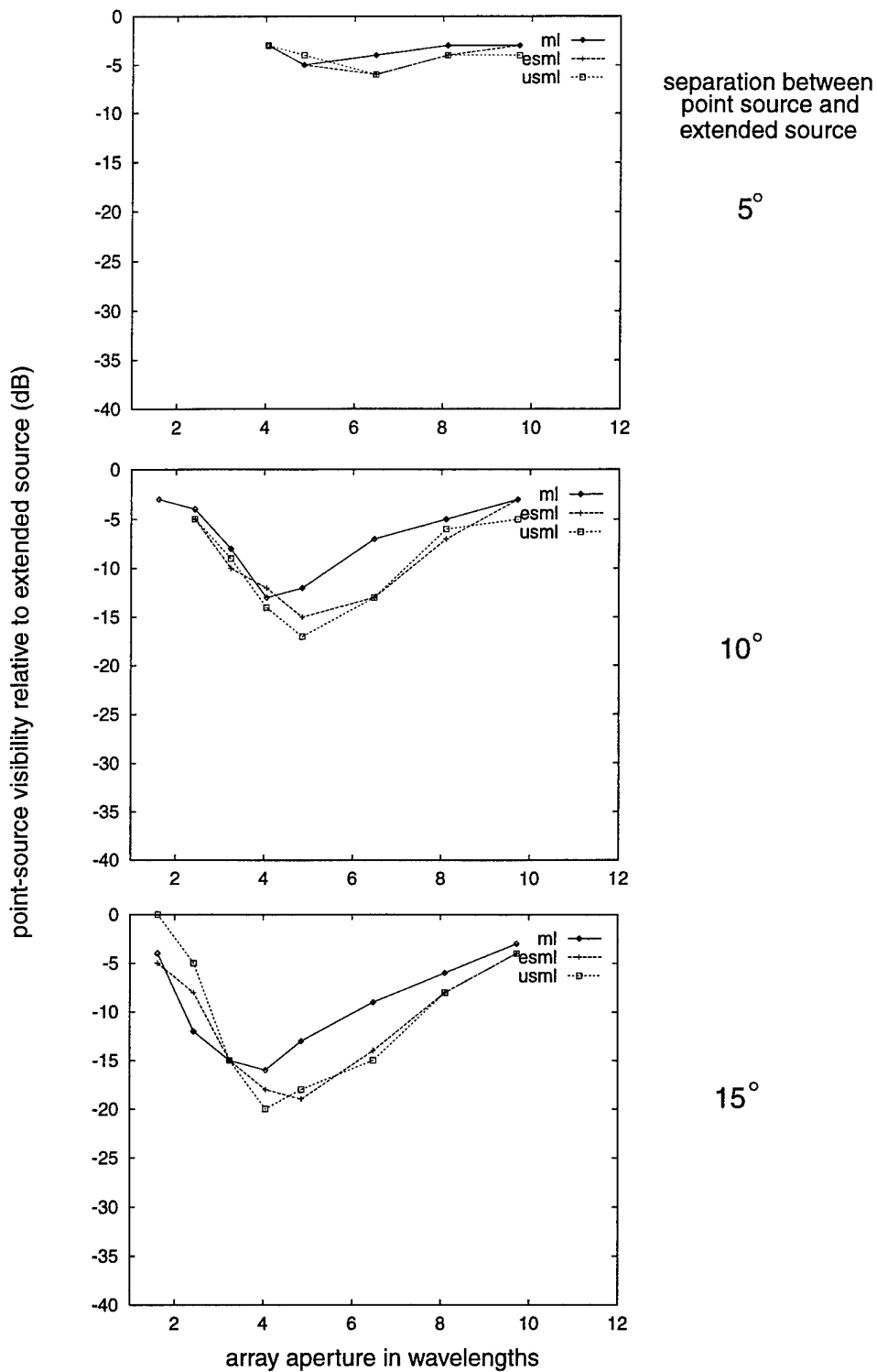


Figure 18. Point-source visibility as a function of array aperture, for the centered-circle array in the presence of large antenna pattern errors, for the three modelled DF techniques: ML, ESML, and USML.

5.0 SUMMARY AND DISCUSSION

The spread maximum-likelihood technique clearly improves DF performance over that of the conventional deterministic maximum-likelihood technique, in terms of point-source visibility, for all four array geometries, with and without pattern errors. These improvements are manifested at array apertures above 4 wavelengths, and in all cases they extend the useful range of array apertures upward.

The two spread maximum-likelihood techniques, ESML and USML are observed in these simulations to be similar in their performances in nearly all cases, despite the fact that only USML represents an exact statistical match between the assumed spread source distributions fitted to the data and the distribution modelled in the data; ESML assumes a significantly different spread distribution. Thus, in applying the SML technique to real data, the issue of whether or not the assumed spread-source distribution shape is a good fit to the actual spread-source distributions present in the data is not important to the success of the technique. Most of the results were found using six assumed signal distributions; it was only when the number of assumed signal distributions was reduced to be equal to the number of distributions present in the data (two) that the assumed distribution shape became an important factor in determining performance. Thus extra assumed directions alleviate the potentially harmful effects of mismatches between assumed and actual distribution shape mismatches.

The previous study [6], which used deterministic maximum likelihood and compared performances of the four array geometries with and without pattern errors, found the star array to perform best. The same is revealed in the present study with the new spread maximum-likelihood technique.

In the absence of pattern errors, the star array achieves remarkably good point-source visibilities, more so than the other arrays. When pattern errors are included, the performance advantage of this array or of the SML algorithm, over the other arrays or the ML algorithm, is reduced. Using the SML algorithm together with the star array improves performance to the point where limits are set mostly by antenna pattern errors, even with large apertures. This finding underscores the importance of knowing the antenna patterns accurately in a high-performance HF DF system.

REFERENCES

- [1] Kelly, M.C., *The Earth's Ionosphere: Plasma Physics and Electrodynamics*, Academic Press, 1989.
- [2] Tsunoda, R.T., *High Latitude F Region Irregularities: A Review and Synthesis*, Rev. Geophys., Vol. 26, No. 4, pp. 719-760, 1987.
- [3] Heppner, J.P., and N.C. Maynard, *Empirical High-Latitude Electric Field Models*, J. Geophys. Res., Vol. 92, No. A5, pp. 4467-4489, 1987.

- [4] Jenkins, R.W., *Preliminary Analysis of Kestrel Data*, informal CRC technical memorandum DRL/TM083/92, 1992.
- [5] Jenkins, R.W., *Modelling Studies of HF Direction Finding in the Presence of Extended Scattering Regions and Sporadic E*, Proc. Symposium on Radiolocation and Direction Finding, Southwest Research Institute, San Antonio Tx., Session 1, Paper 1, 1995.
- [6] Jenkins, R.W., *The Effects of Antenna Array Geometry and Element Pattern Uncertainty on High-Latitude HF Direction Finding*, CRC Report 97-006, 1997.
- [7] Read, W., personal communication, 1997.
- [8] Jenkins, R.W., *A Comparison of Modelled and Measured HF Antenna Array Patterns*, CRC Tech. Note 96-002, 1996.
- [9] Dumas, D., *Direction-Finding Algorithms and Software for a Sampled-Aperture Antenna Array Operating at High Latitudes in the HF Band*, CRC informal technical memorandum VPRB 03/98, 1998.

UNCLASSIFIED

SECURITY CLASSIFICATION OF FORM
(highest classification of Title, Abstract, Keywords)

DOCUMENT CONTROL DATA

(Security classification of title, body of abstract and indexing annotation must be entered when the overall document is classified)

1. ORIGINATOR (the name and address of the organization preparing the document. Organizations for whom the document was prepared, e.g. Establishment sponsoring a contractor's report, or tasking agency, are entered in Section 8) Communications Research Centre 3701 Carling Avenue P.O. Box 11490, Station H Ottawa, Ontario Canada K2H 8S2		2. SECURITY CLASSIFICATION (overall security classification of the document including special terms if applicable) UNCLASSIFIED	
3. TITLE (the complete document title as indicated on the title page. Its classification should be indicated by the appropriate abbreviation (S,C,R or U) in parentheses after the title) A comparison of spread and point-source multiple-direction estimation techniques for high latitude HF direction-finding (U).			
4. AUTHORS (Last name, first name, Middle initial) Robert W. Jenkins			
5. DATE OF PUBLICATION (month and year of publication of document) April 1998	6a. NO. OF PAGES (total containing information. Include Annexes, Appendices, etc.) 31	6b. NO. OF REFS. (total cited in document) 9	
7. DESCRIPTIVE NOTES (the category of the document, e.g. technical report, technical note or memorandum. If appropriate, enter the type of report, e.g. interim, progress, summary, annual or final. Give the inclusive dates when a specific reporting period is covered.) CRC-TN-98-002			
8. SPONSORING ACTIVITY (the name of the department project office or laboratory sponsoring the research and development. Include the address.) Defence Research Establishment Ottawa(DREO) 3701 Carling Avenue Ottawa, Ontario K1A 0Z2			
9a. PROJECT OR GRANT NO. (if appropriate, the applicable research and development project or grant number under which the document was written. Please specify whether project or grant) 661-990-X77-998445419-(276870)-WK UNIT #5bd14		9b. CONTRACT NO. (if appropriate, the applicable number under which the document was written)	
10a. ORIGINATOR'S DOCUMENT NUMBER (the official document number by which the document is identified by the originating activity. This number must be unique to this document) CRC TN 98-002		10b. OTHER DOCUMENT NOS. (Any other numbers which may be assigned to this document either by the originator or the sponsor)	
11. DOCUMENT AVAILABILITY (any limitations on further dissemination of the document, other than those imposed by security classification) <input checked="" type="checkbox"/> Unlimited distribution <input type="checkbox"/> Distribution limited to defence departments and defence contractors; further distribution only as approved <input type="checkbox"/> Distribution limited to defence departments and Canadian defence contractors; further distribution only as approved <input type="checkbox"/> Distribution limited to government departments and agencies; further distribution only as approved <input type="checkbox"/> Distribution limited to defence departments; further distribution only as approved <input type="checkbox"/> Other (please specify)			
12. DOCUMENT ANNOUNCEMENT (any limitation to the bibliographic announcement of this document. This will normally correspond to the Document Availability (11). However, where further distribution (beyond the audience specified in 11) is possible, a wider announcement audience may be selected.) UNLIMITED			

UNCLASSIFIED

SECURITY CLASSIFICATION OF FORM

SECURITY CLASSIFICATION OF FORM
(highest classification of Title, Abstract, Keywords)

13. **ABSTRACT** (a brief and factual summary of the document. It may also appear elsewhere in the body of the document itself. It is highly desirable that the abstract of classified documents be unclassified. Each paragraph of the abstract shall begin with an indication of the security classification of the information in the paragraph (unless the document itself is unclassified) represented as (S), (C), (R), or (U). It is not necessary to include here abstracts in both official languages unless the text is bilingual).

Previous simulation studies were conducted to determine the direction-finding performance of four different antenna array geometries with and without antenna pattern errors, operating with the deterministic maximum likelihood (ML) algorithm. Here they are extended to a new DF algorithm, spread maximum likelihood (SML), which assumes distributions of signal directions, rather than single directions, to approximate the signal information seen by the array. The SML algorithm is thought to be more appropriate to the high-latitude HF radio environment, where signals often arrive from a spread set of directions, due to multiple reflections or scattering from irregularities in the ionosphere and, at the same time, from a single great-circle direction as a results of sporadic E propagation. Using a performance criterion of 'point-source visibility' in the presence of a stronger spread source, the simulation shows the SML technique to yield substantially better performance than ML, for all arrays and levels of error, and array apertures of four wavelengths or more. SML technique extended the useful range of array apertures upwards to 10 wavelengths in most cases. As was seen previously for the ML algorithm, the a three-pronged star configuration was found to be best of the array geometries tested.

14. **KEYWORDS, DESCRIPTORS or IDENTIFIERS** (technically meaningful terms or short phrases that characterize a document and could be helpful in cataloguing the document. They should be selected so that no security classification is required. Identifiers, such as equipment model designation, trade name, military project code name, geographic location may also be included. If possible keywords should be selected from a published thesaurus, e.g. Thesaurus of Scientific Terms (TEST) and that thesaurus-identified. If it is not possible to select indexing terms which are Unclassified, the classification of each should be indicated as with the title.)

HF Radio
HF Direction-Finding
Direction-Finding Techniques
High Latitude HF Radio Propagation
HF Antenna Patterns
HF Antenna Arrays
Antenna Pattern Errors